



Original Paper

# Experimental Investigation of Mechanical Properties and Failure Behavior of Fluid-Saturated Hot Dry Rocks

Daobing Wang<sup>1,3</sup>, Xiaobing Bian<sup>2,3</sup>, Hao Qin<sup>1</sup>, Dongliang Sun<sup>1</sup> and Bo Yu<sup>1,3</sup>

Received 31 August 2020; accepted 22 September 2020  
Published online: 9 October 2020

Thousands of cubic meters of fluid are continuously injected for a long term to create complex fracture patterns in hydraulic fracturing of hot dry rocks. However, the physics and mechanics behind the interaction of fluid–rock are not fully understood at present. To reveal the related damage mechanisms of saturated rock samples such as damage initiation and evolution at various alternative stress levels, a series of in-house laboratory tests were performed on a TAW-series triaxial rock mechanics testing system, combined with ultrasound measurement and acoustic emission (AE) monitoring. After saturation with nano-emulsion and distilled water, ultrasound velocity of longitudinal wave was increased by 40%. Saturation weakens these mechanical parameters such as the crack damage stress ratio, fracture toughness and cohesive strength under different stress conditions. Fluid-saturated rock sample has higher AE hit rate than dry rock sample. Meanwhile, many step-like jumps appeared on the curve of cumulative AE events. Failure envelop, *b*-value and frequency spectrum were analyzed out to compare the mechanical difference between fluid-saturated and dry rock samples. The experimental results demonstrate that the saturation increased the pore pressure in rocks and further promoted crack propagation in hydraulic fracturing. Moreover, nano-emulsion liquid is more advantageous than distilled water for enhancing fracture complexity. This investigation provides for better understanding of the mechanisms of complex fracture formation in deep geothermal reservoirs.

**KEY WORDS:** Hot dry rock, Rock mechanics, Experimental study, Acoustic emission, Hydraulic fracturing.

## INTRODUCTION

Hot dry rock is a kind of igneous or metamorphic rock with a temperature higher than 200 °C. Burial depth of hot dry rocks is normally between 3

and 10 km, with little or no fluid inside (Wan et al. 2005; Yang et al. 2019). The thermal energy stored in hot dry rock in China is equivalent to about 856 trillion tons of standard coal energy (Gong et al. 2020), which accounts for about 16% of the world's energy resources. Thus, hot dry rock is expected to become a strategic alternative energy source.

Hydraulic fracturing treatment is a key technology to extract deep-subsurface geothermal energy (Jupe et al. 1992; Wang et al. 2019a, b, c; Zhang et al. 2019; Wang et al. 2020a, b, c, d). Generally, a large volume of fracturing fluid is continuously injected to high-temperature rock mass for several days, reported in the project of enhanced geother-

<sup>1</sup>School of Mechanical Engineering, Beijing Key Laboratory of Pipeline Critical Technology and Equipment for Deep Water Oil and Gas Development, Beijing Institute of Petrochemical Technology, Beijing 102617, China.

<sup>2</sup>Sinopec Research Institute of Petroleum Engineering, Beijing 100101, China.

<sup>3</sup>To whom correspondence should be addressed; e-mail: upcwdb@bjpt.edu.cn, xiaobingbian@126.com, yubobox@vip.163.com

mal system in Europe and the USA, such as the 2006 Basel Project in Switzerland (Mignan et al. 2015; Xie et al. 2015). It follows that water–rock interaction is widely present in hydraulic fracturing of geothermal reservoirs. Therefore, it is a key problem to investigate the mechanical properties and rupture mechanisms of water-saturated hot dry rocks.

The interaction between fluid and hot dry rocks mainly involves physical effect, mechanical effect and chemical effect (Althaus et al. 1994; Zhang et al. 2018; Hasan et al. 2019). The variation of temperature caused by cold water injection is a typical physical process, which brings about the effect of thermal stress cracking in hot dry rocks (Gringarten et al. 1975; Bauer and Handin 1983; Kohl et al. 1995). In the past decades, many rock mechanics experiments have been performed to investigate deformation behavior at various temperatures (Menéndez et al. 1999; Chaki et al. 2008; Yu et al. 2015). These investigations showed that thermal stress, variation of mineral composition and microstructure at high temperature cause the variation of rock mechanics characters and degradation of hot dry rocks (Zhang et al. 2014; Yu et al. 2015). The transition from elastic deformation to elastic–plastic deformation is usually observed from the stress–strain response as temperature increases (Yang et al. 2017; Wang et al. 2019a, b, c). When the temperature is beyond a critical value, mechanical parameters such as elastic moduli, failure strength and stress level at the onset of dilation decrease sharply and the permeability increases dramatically (Chaki et al. 2008). In addition, the phase change of quartz occurs at 573 °C. Meanwhile, acoustic emission (AE) monitoring showed that frequent thermal cracking appears in the pre-peak period (Yang et al. 2017). Microstructure analyses demonstrated that several micro-fractures with short lengths and narrow apertures are formed in hot dry rocks after the above-mentioned critical value of temperature (Bauer and Handin 1983; Zhang et al. 2018; Wang et al. 2020a, b, c, d). Moreover, our semicircular bend test showed that new artificial crack does not initiate from an initial predefined crack and propagates along a different direction from the predefined crack path (Wang et al. 2019a, b, c).

During the exploitation of geothermal reservoirs, water is flowed cyclically through hydraulic fractures to achieve the heat exchange with hot rock matrix (Richards et al. 1992; Evans et al. 2005; Hasan et al. 2019; Guo et al. 2019). The chemical interactions between water and hot dry rock appear

in the forms of mineral dissolution, substitution and precipitation, which affect the development of geothermal energy (Zhao et al. 2020). The main factors of those chemical interactions include the circulation rate of aqueous solution, the mineral composition of rocks and the chemical properties of aqueous solution (Bai et al. 2012; Guo et al. 2015; Zhao et al. 2020). Experimental results showed that aqueous solutions with too high or too low pH can damage the structure or composition of hot dry rocks, leading to variation in physical property (Pauwels et al. 1992; Bai et al. 2012). Field operations in borehole GPK1 in Soultz-sous-Forêts (Pauwels et al. 1992) showed that dissolution of minerals such as biotite was very fast in the first 100 min and then decreased after a few minutes.

Besides the physical and chemical effects of water–rock interaction, our previous study showed that fluid can alter the rock mechanical properties and the associated fracture network patterns in brittle shale (Wang et al. 2020a, b). Different from clay-rich and organic matter-rich shale, hot dry rock is usually an igneous rock that is rich in quartz and feldspar. To investigate the rupture mechanisms of fluid-saturated hot dry rocks, a series of in-house laboratory investigation was performed on servo-controlled triaxial rock mechanics testing system combined with AE monitoring. The associated mechanical behavior of hot dry rock with saturated fluid at different stress levels were also analyzed in detail. This investigation provides new insights into enhancing the thermal extraction efficiency in geothermal reservoirs.

## MATERIALS AND METHODS

### Rock Sample

As shown in Figure 1a, a grayish white granite rock outcrop (Wang et al. 2019a, b, c) from Yan-jiao town, Hebei Province, north China, was drilled to cylindrical samples (25 mm × 50 mm), according to the suggested standard in rock mechanics. Both ends of a specimen were fine-ground and polished to produce a smooth surface with minimum friction during triaxial compression tests. Before the rock mechanics experiment, the granite samples were placed in a drying oven at a constant temperature of 90 °C. Then, the specimens were saturated with distilled water and nano-emulsion fluid for seven days (Fig. 1b). The saturated-fluid granite samples were compared with a dry sample during the

experiment. The rock permeability varied between 0.00095 and 0.0012 md and the porosity ranged from 1.22 to 3.43%, showing that the granite specimens were very tight.

Fracture toughness ( $K_{IC}$ ) is an important fracture mechanics parameter, which characterizes the ability of rocks to prevent crack propagation in hydraulic fracturing (Atkinson 1987). To obtain fracture toughness of saturated-fluid hot dry rocks, semicircular bending test (ASTM D8044-16 2016; Nejati et al. 2019; Wang et al. 2019a, b, c) was conducted on a triaxial apparatus. The granite sample was processed into a semicircular disk specimen with 40 mm radius and 35 mm thickness. An initial crack with 20 mm length and 2 mm width was pre-cast in the middle of specimen. The initial crack was normal to the bottom edge of specimen (Fig. 2). Similar to the above-mentioned saturated method, these semicircular specimens were immersed in the fluids for seven days before semicircular bending test.

**Experimental Setup**

A TAW-2000 electro-hydraulic servo-controlled rock triaxial testing machine was utilized to



**Figure 1.** Samples: (a) cylindrical rock samples; and (b) saturated-fluid-rock samples.

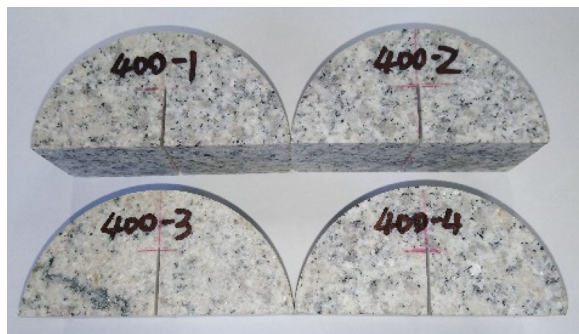


**Figure 2.** Semicircular disk specimen.

perform the conventional triaxial compression test (Fig. 3). The TAW-2000 triaxial apparatus is supplied by Changchun Chaoyang Testing Instrument Co., Ltd. in northeast China. This testing apparatus can provide a compressional load capacity up to 2000 kN, maximum pore pressure up to 70 MPa and maximum confining pressure up to 140 MPa (Wang et al. 2020a, b). The axial and radial strains were measured by an extensometer named as YSZ-50. The specimen was wrapped within a heat-shrinkable tube in order to apply a confining pressure on the lateral of specimen.

The ultrasound velocity measurement system (Fig. 4) is composed of an electric pulser-receiver (Olympus 5077PR), an oscilloscope and a pair of sensors (Nano-30). The longitudinal wave sensors were kept close to each end of specimen. To improve the contact effect between each end of specimen and each sensor, a special acoustic couplant was uniformly coated on each face of sensor (Wang et al. 2015a, b).

The PCI-2 system was used to real-time synchronous monitor AE event, which is supplied by Physical Acoustic Corporation (PAC). This AE system has the quality of full waveform acquisition (Wang et al. 2020a, b) and adopts an 18-bit analog-to-digital (A/D) converter technique with broadband response between 100 and 1000 kHz. The electrical signals from each sensor were amplified by a low noise preamplifier at a 40 dB threshold level (Lockner 1993). The filter bandwidths were set between 20 kHz and 3 MHz to improve measurement precisions (Lockner 1993). This AE system can record AE parameters up to 20, including, among others, ring counts, energy, peak frequency and amplitude.

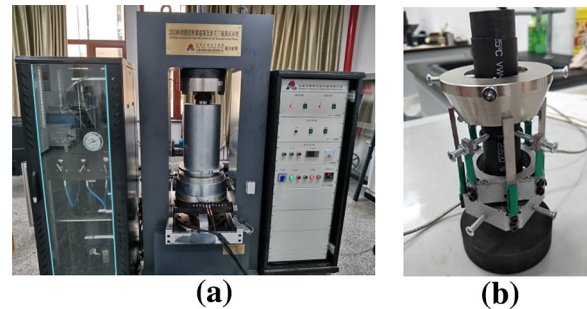


**Figure 3.** TAW-2000 triaxial testing machine: (a) triaxial cell; (b) YSZ-50 extensometer.

**Experimental Methods**

The saturated-fluid granite samples were compressed by applying an axial load from TAW-2000 apparatus with a 0.04 mm/min displacement rate under uniaxial and triaxial stress conditions, respectively, compared to the dry granite samples. For each specimen, the confining pressure was assigned as 0 MPa, 6 MPa, 25 MPa or 50 MPa in order to determine the failure envelope in rock mechanics. At the same time, the AE feature was also monitored during the compression test. From the stress-strain curve of rock samples, the volumetric strain was determined by the sum of the axial strain and twice the radial strain(Fjar et al. 2008), thus:

$$\varepsilon_v = \varepsilon_a + 2\varepsilon_r, \tag{1}$$

where  $\varepsilon_v$  is volumetric strain,  $\varepsilon_a$  is axial strain, and  $\varepsilon_r$  is circumferential strain. As shown in Figure 5, crack damage stress  $\sigma_{cd}$  can be determined as the axial stress at the deflection point of volumetric strain, where a rock sample is at the onset of dilatancy (Wang et al. 2020a; Zhuang et al. 2020).

In the experiment of semicircular bending test, a concentrated load force was imposed on the top of semicircular specimen at a 0.04 mm/min displacement rate. The AE feature was also monitored at the same time (Fig. 6). Once the loading force exceeded a specific value, the artificial crack grew along the pre-defined path of the initial crack, as expected. The relationship curve of displacement vs. axial force can be derived from the semicircular bending test. Based on the experimental result, the fracture toughness  $K_{IC}$  can be calculated as (Dai et al. 2015; Wang et al. 2019a, b, c):

$$K_{IC} = \frac{P_{max}\sqrt{\pi a}}{2RB} Y^* \tag{2}$$

$$Y^* = -1.297 + 9.516 \frac{S}{2R} - \left(0.47 + 16.457 \frac{S}{2R}\right) \cdot \frac{a}{R} + \left(1.071 + 34.401 \frac{S}{2R}\right) \cdot \left(\frac{a}{R}\right)^2, \tag{3}$$

where  $K_{IC}$  is the mode-I fracture toughness of specimen,  $P_{max}$  is peak value of axial load in the

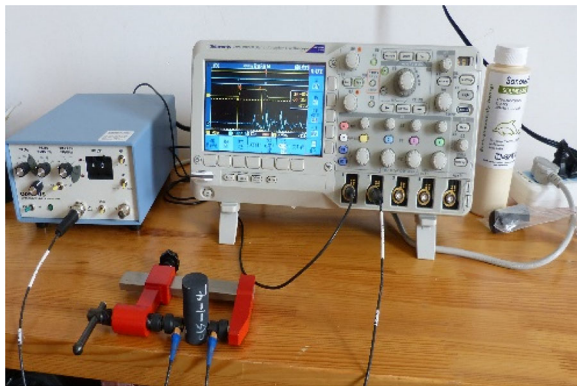


Figure 4. Ultrasound velocity measurement system (Wang et al. 2015b).

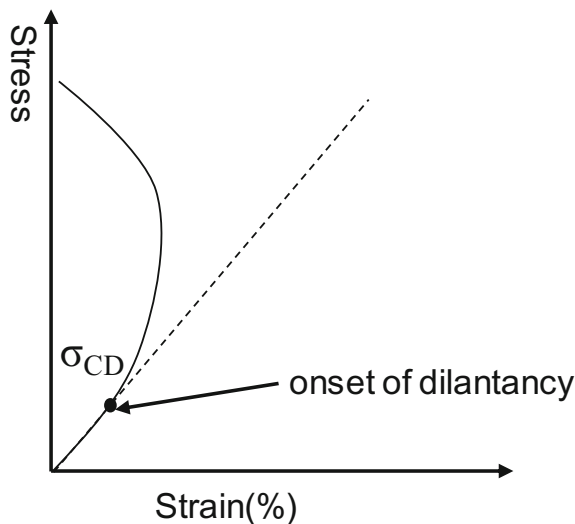


Figure 5. Determination method for crack damage stress  $\sigma_{cd}$  from volumetric strain curve.



Figure 6. Semicircular bending test via the TAW-2000 series triaxial apparatus.

semicircular bending test,  $Y^*$  is the dimensionless coefficient,  $R$  is radius of semicircular specimen,  $S$  is distance between two supporting point on the bottom edge, which maintains a constant value of 38 mm in the experiment, and  $B$  is thickness of semicircular specimen.

**EXPERIMENTAL RESULTS**

**Longitudinal Wave Velocity**

Ultrasound velocity can effectively detect variation of pore structure in rocks (Nur and Simmons 1969; Kahraman 2007; Wang et al. 2015a, b). The longitudinal wave velocities ( $V_p$ ) of fluid-saturated hot dry rock samples were measured and compared with the ultrasound velocity of dry samples (Fig. 7). This figure shows that  $V_p$  of fluid-saturated samples was 30–50% higher than that of dry samples. This result is consistent with the previous studies of granite samples. Kahraman (2007) conducted experimental investigation of eight different types of

granite samples with porosity in the range of 0.35–3.59%. It merits mentioning that the variation of  $V_p$  induced by water saturation in low-porosity samples (generally less than 1%) is much greater than that in high-porosity samples.

The increase percentage of longitudinal wave velocity is defined as:

$$\Delta V/V = \frac{V_{p,saturated} - V_{p,dry}}{V_{p,dry}}, \quad (4)$$

where  $\Delta V/V$  is the increase percentage of ultrasound velocity,  $V_{p,dry}$  is ultrasound velocity of dry samples, and  $V_{p,saturated}$  is ultrasound velocity of saturated samples. The results of  $\Delta V/V$  of different fluid-saturated samples are listed in Table 1, compared with the ultrasound velocity of dry samples. We observed that the variation range of nano-emulsion saturated samples was between 53.5 and 67.9%, and the variation of distilled water-saturated samples ranged from 48.1 to 61.3%. Thus, we can deduce that the increase ratio of ultrasound velocity saturated by nano-emulsion is greater than that saturated by

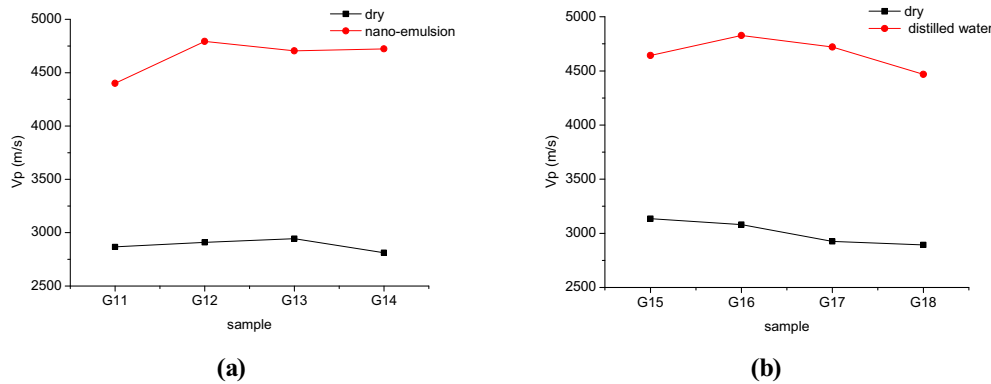


**Figure 7.** Comparison of ultrasound velocity  $V_p$  between dry samples and samples saturated with (a) nano-emulsion and (b) distilled water.

**Table 1.** Comparison of increased proportion of velocity between dry and fluid-saturated samples

Sample	$V_{p,dry}$ (m/s)	$V_{p,saturated}$ (m/s)	Fluid type	$\Delta V/V$ (%)
G11	2866	4400	Nano-emulsion	53.5
G12	2909	4793		64.8
G13	2944	4705		59.8
G14	2812	4723		67.9
G15	3134	4644	Distilled water	48.1
G16	3080	4828		56.7
G17	2926	4720		61.3
G18	2894	4470		54.5

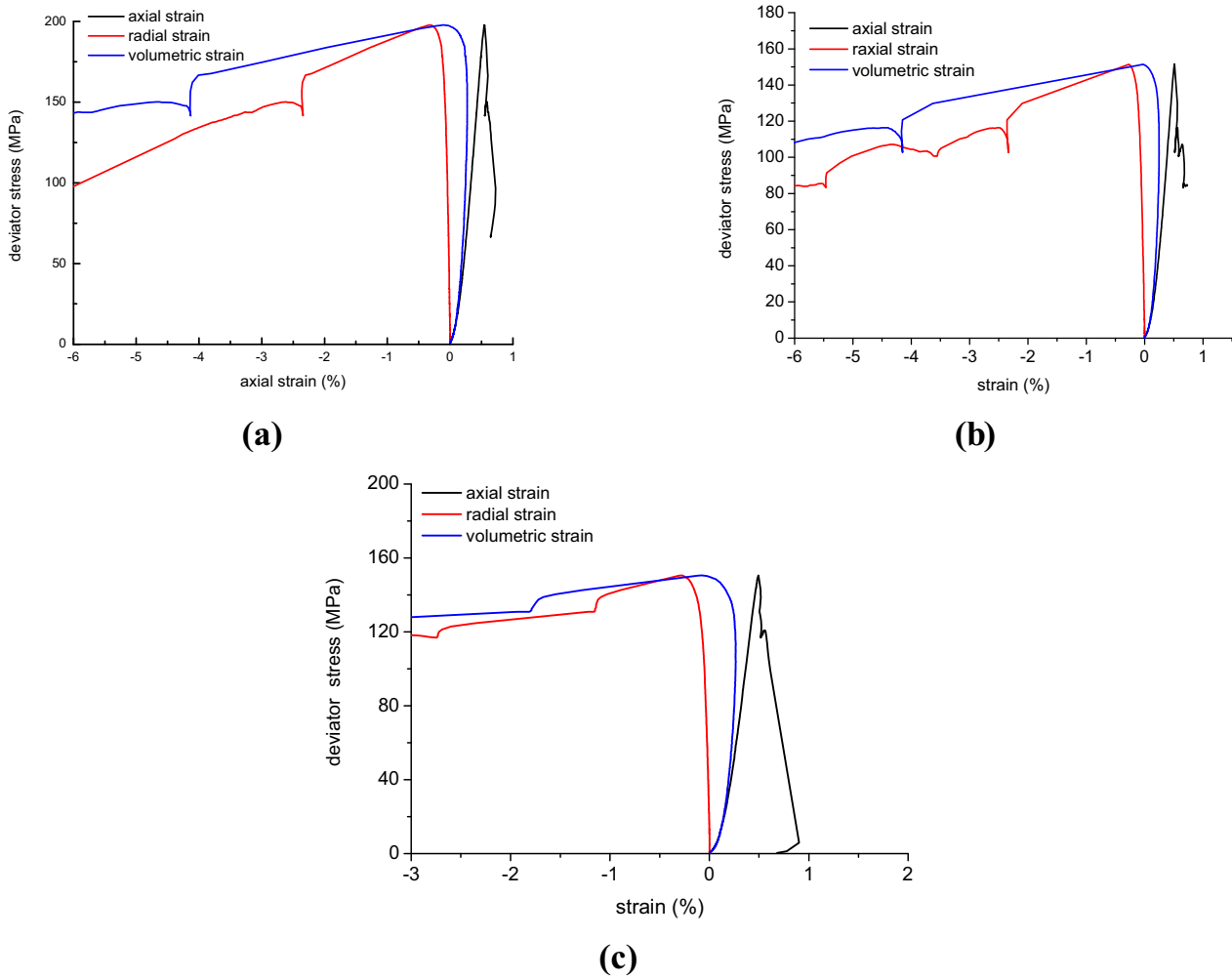


**Figure 8.** Deformation behavior of rock samples under uniaxial stress conditions ( $P_c = 0$  MPa): (a) dry; (b) saturated with nano-emulsion; (c) saturated with distilled water.

distilled water. This is because nano-emulsion can enter into micro-nano-pores in rocks samples easier than distilled water. Variations in  $V_p$  are a good reflection of water absorption in hot dry rocks. In the next analysis, we report that the ultrasound velocity significantly affects AE characteristics of hot dry rock samples.

### Rock Deformation and Mechanical Parameters

Under uniaxial stress conditions, the deformation behavior of fluid-saturated samples is shown in Figure 8. We observed that fluid-saturated and dry samples were characterized mainly by brittle deformation. There was no obvious difference of stress–

strain curves between fluid-saturated and dry samples. However, the uniaxial compressive strength (UCS) of fluid-saturated samples was lower than that of dry samples. This indicates that fluid can weaken the mechanical strength of hot dry rocks. Our result is in accordance with the previous study by Zhou et al. (2016). They observed that free water inside rock samples increases pore pressure. The increased pressure can further boost crack initiation and propagation, and therefore, the failure strength of specimen is significantly reduced (Zhou et al. 2016). In addition, fluid saturation can weaken the cementation strength between mineral grains in rocks and, thus, results in a lower failure strength (Zhuang et al. 2020).

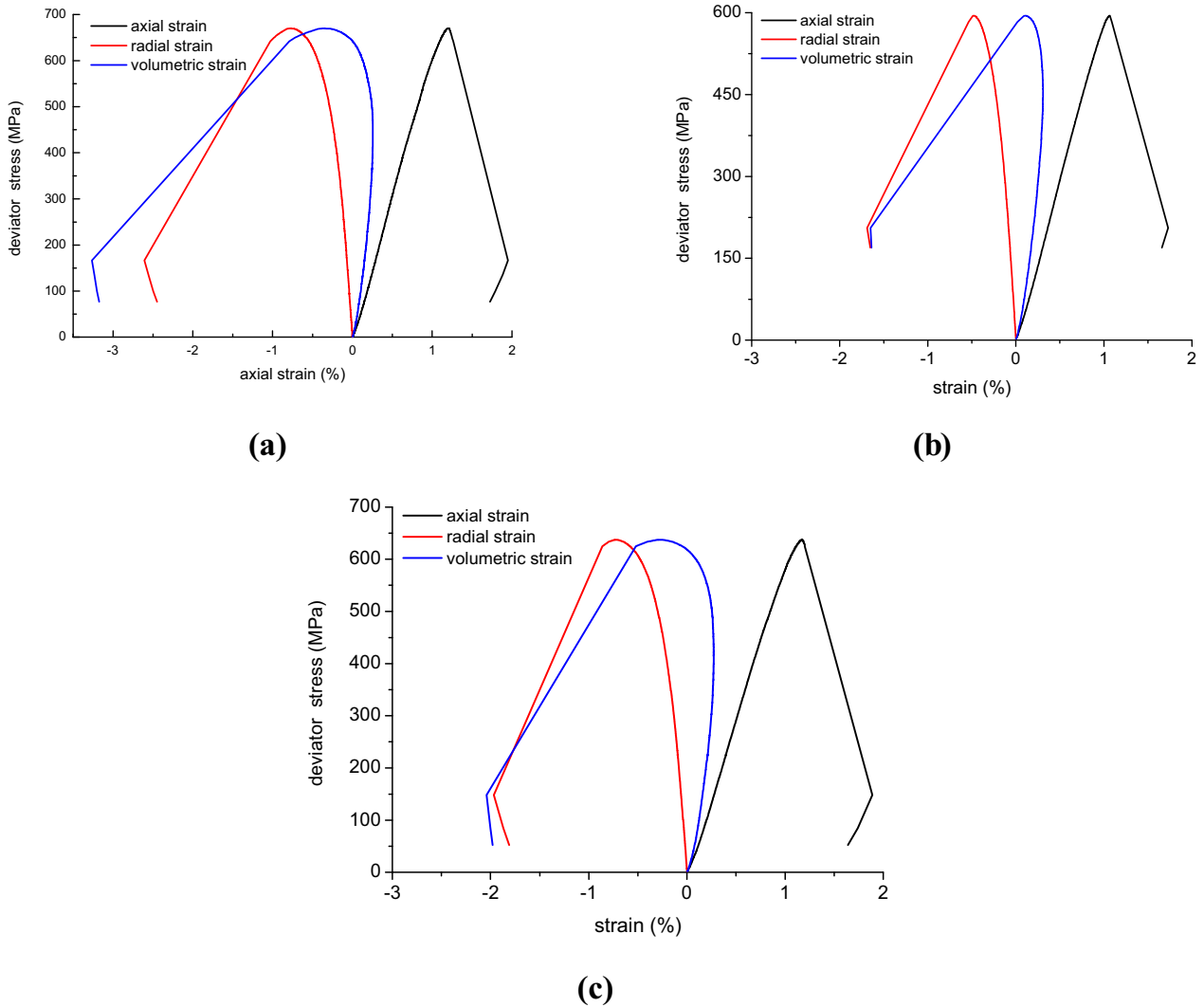


**Figure 9.** Deformation behavior of rock samples under triaxial stress conditions ( $P_c = 50$  MPa): (a) dry; (b) saturated with nano-emulsion; (c) saturated with distilled water.

When a confining pressure ( $P_c$ ) of 50 MPa was applied on fluid-saturated samples, the stress–strain curves are shown in Figure 9. This figure shows that plastic deformation occurred on the stress–strain curves under triaxial stress conditions. There was an obvious deflection point of volumetric strain curves, while the deflection point was difficult to observe under uniaxial stress conditions. As previously described, this deflection point showed that rock damage initiated in rock samples. Beyond the level of damage stress, rock deformation shifts from brittle behavior to plastic behavior. Similar to the results under uniaxial loading, we could not identify

the difference of stress–strain curves between fluid-saturated and dry samples. The failure strength of fluid-saturated samples was also lower than that of dry samples, indicating that the mechanical strength of hot dry rocks is affected by fluid saturation. This variation is in accordance with the result of the increase ratio of ultrasound velocity in “Longitudinal Wave Velocity” section.

Based on the stress–strain data, some key mechanical parameters such as elastic moduli, compression strength and damage stress were obtained. The crack damage stress ratio is defined as the ratio of  $\sigma_{cd}$  to compression strength at different

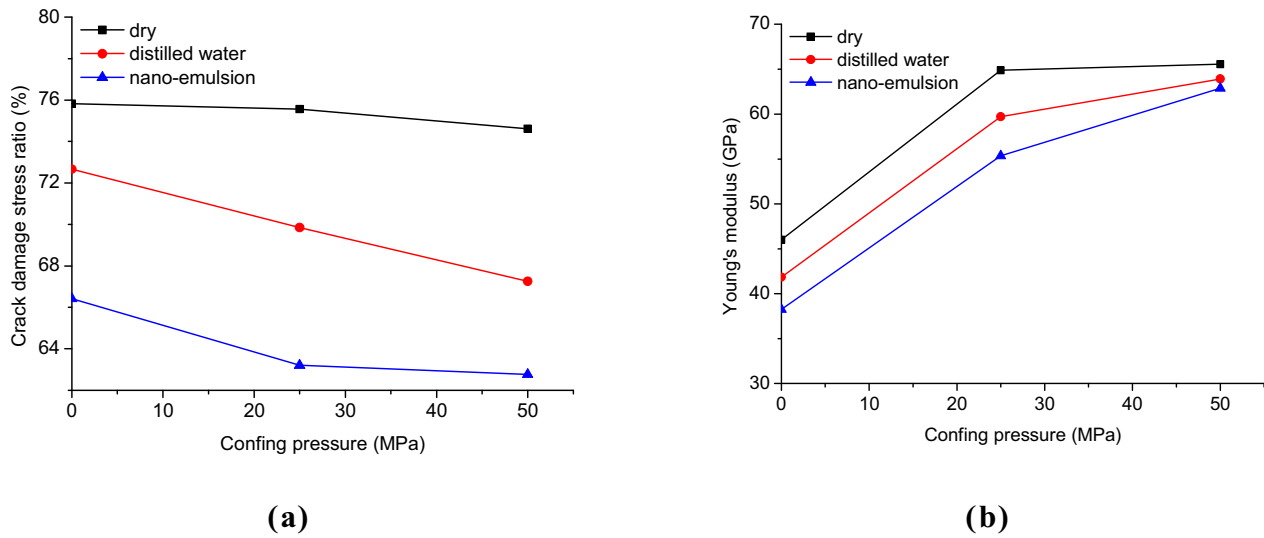


**Figure 10.** Comparison of mechanical parameters between fluid-saturated and dry rock samples: (a) crack damage stress ratio; (b) elastic moduli.

confining pressures (Zhuang et al. 2020), which corresponds to the long-term rock strength. Figure 10 shows these mechanical parameters of fluid-saturated and dry samples at different confining pressures. We observed that the mean crack damage stress ratio for fluid-saturated samples was about 4% less than that for dry samples. Previous studies reported that the value of crack damage stress ratios decrease by 2.2–3.1% upon fluid saturation, which indicates rock failure for fluid-saturated samples was slightly earlier than that for dry samples (Zhuang et al. 2020). In rock mechanics, the crack damage stress ratio is normally in the range of 71–84% for various kinds of granite samples (Cai et al. 2004; Zhuang et al. 2020). Thus, our result is in line with the previous studies. In addition, the crack damage stress ratio for nano-emulsion saturated samples was about 4–8% less than those for samples saturated with distilled water, indicating that nano-emulsion fills preexisting micro-cracks in rock samples easier than distilled water. Similarly, elastic moduli between fluid-saturated and dry samples have the same variation trend as that of the crack damage stress ratios (Fig. 10b). Thus, fluid saturation can weaken mechanical parameters of rock.

### Acoustic Emission Characteristics

Both AE hit rate and cumulative ringing count represent frequency and intensity of AE signals, and

characterize the intensity of AE activity (Lockner 1993). AE rate denotes number of AE events per unit time. Figure 11 presents AE hit rate and cumulative AE ringing count curves of specimens under uniaxial stress conditions. We observed that dry sample generated less cumulative AE ringing count before peak stress, and several AE ringing counts appeared once the stress level was up to UCS. Compared with dry sample, fluid-saturated samples have more steps on the curve of cumulative AE ringing counts. These steps show that fluid saturation can promote micro-crack initiation, propagation and nucleation in rock samples. Zhuang et al. (2020) reported that the maximum AE hit rate for saturated samples was much higher than for dry samples. This result is in accordance with our results shown in Figures 11 and 12. We observed that AE hit rate and AE energy have the same variation trend for each sample. Figures 11a and 12a show a relatively quiet period after 425 s on the curves of the dry sample, and the fluid-saturated sample had higher AE energy and AE hit rate than the dry sample.

Compared with uniaxial stress conditions, cumulative AE ringing counts under triaxial stress conditions decreased by 10% due to the action of confining pressure (Fig. 13). We observed that cumulative AE ringing count of dry sample was more than that of saturated samples. There was no significant difference in the cumulative AE ringing count between for dry and fluid-saturated samples.



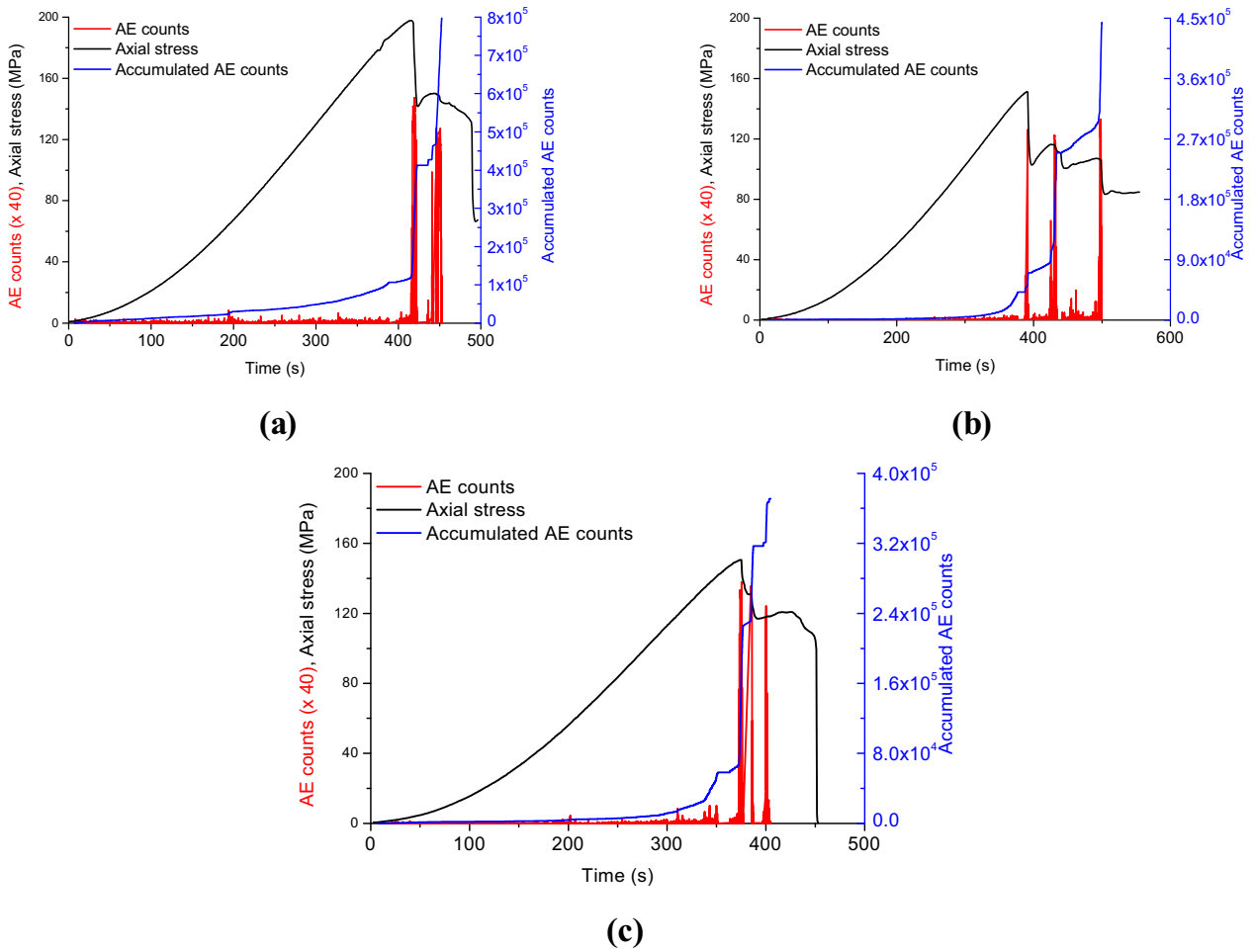


**Figure 11.** AE hit rate and cumulative AE ringing count curves of rock samples under uniaxial stress conditions ( $P_c = 0$  MPa): (a) dry; (b) saturated with nano-emulsion; (c) saturated with distilled water.

However, the dry sample had higher AE hit rate and AE energy in the early stage of loading compared to those of the fluid-saturated samples (Figs. 13 and 14). This variation indicates that fluid can restrain the generation of AE events during the early loading process, and maybe the released AE energy inside samples is absorbed by saturated fluid. However, fluid can promote micro-crack propagation and coalescence under triaxial stress because mechanical parameters such as elastic moduli and crack damage stress ratio decrease (Fig. 10).

### Fracture Toughness

Fracture toughness is a very important fracture mechanics parameter, which is the critical stress

intensity factor of a sharp crack where propagation of the crack suddenly becomes rapid and unlimited (Atkinson 1987). In this study, we tested mode-I fracture toughness parameter  $K_{IC}$  between saturated and dry samples at different temperatures. Figure 15 shows that the value of  $K_{IC}$  for saturated sample was less than that for dry sample at each temperature level due to the weakening effect induced by fluid. We also observed that fracture toughness of nano-emulsion saturated sample was less than that of distilled water-saturated sample, which is in accordance with the results in Figure 8. As previously explained, this is because nano-emulsion fills pre-existing micro-cracks in rock samples much easier than distilled water.

Figure 16 presents the corresponding fracture morphologies between fluid-saturated and dry sam-

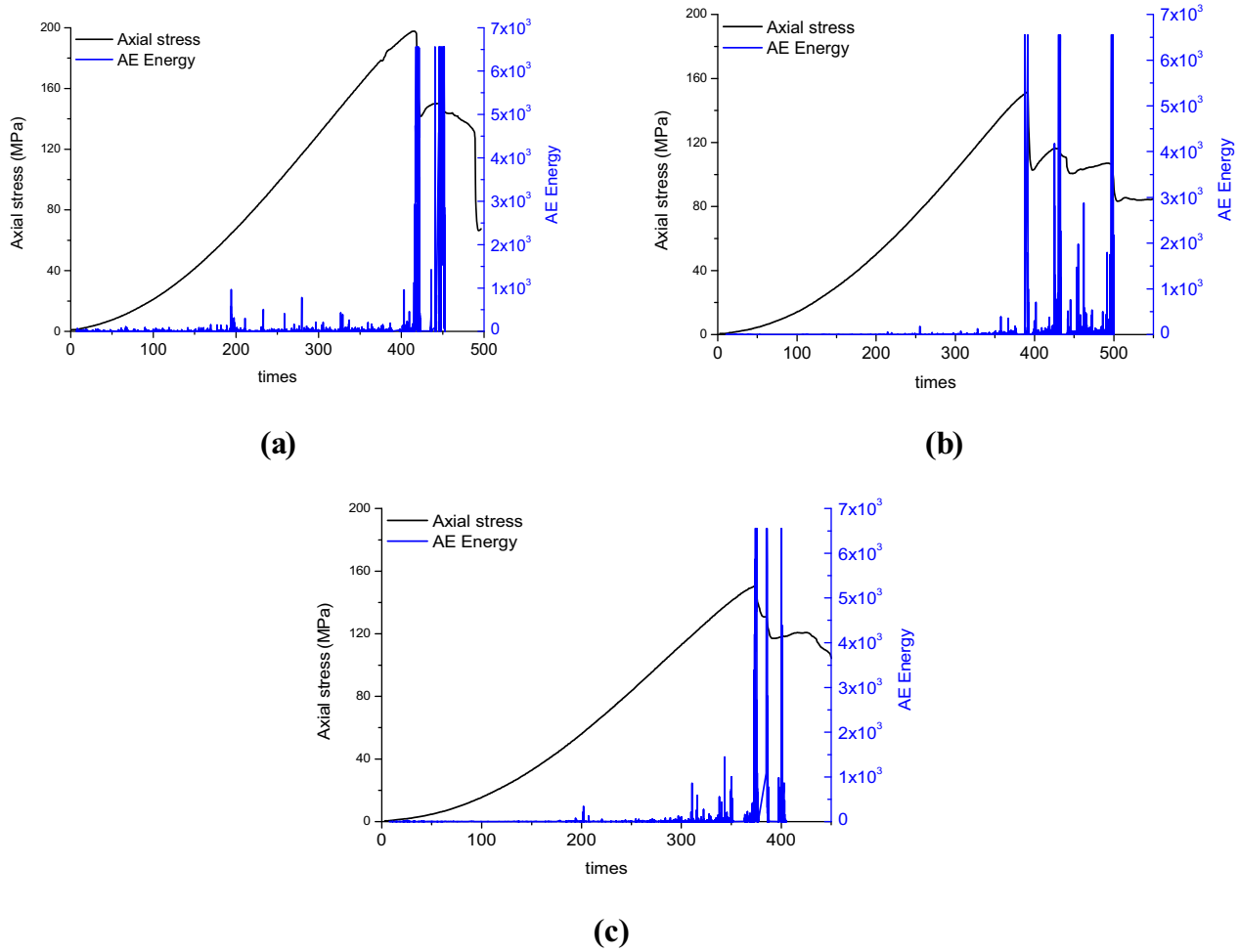


**Figure 12.** AE energy curves of rock samples under uniaxial stress conditions ( $P_c = 0$  MPa): (a) dry; (b) saturated with nano-emulsion; (c) saturated with distilled water.

ples. For dry sample, the artificial crack propagated along the initial crack. However, compared with fracture patterns in the dry sample, more complex fracture patterns were formed in fluid-saturated samples (Fig. 16b, c, and d). The artificial crack initiated from a new direction, which was different from the direction of initial predefined crack due to the combined action of fluid and temperature. Therefore, mechanical interaction between fluid and rocks can enhance fracture complexity in hydraulic fracturing of hot dry rocks. In addition, nano-emulsion saturated samples have more complex fracture complexity than distilled water-saturated samples.

## DISCUSSION

### Failure Envelope

The Mohr–Coulomb criterion, which is widely used in rock mechanics and rock engineering, defines a failure envelope as (Fjar et al. 2008):

$$\tau = \sigma_n \tan(\phi) + c, \quad (5)$$

where  $\tau$  denotes shear stress along the plane of weakness,  $\sigma_n$  denotes normal stress on the plane of weakness,  $c$  denotes cohesion of the rock, and  $\phi$

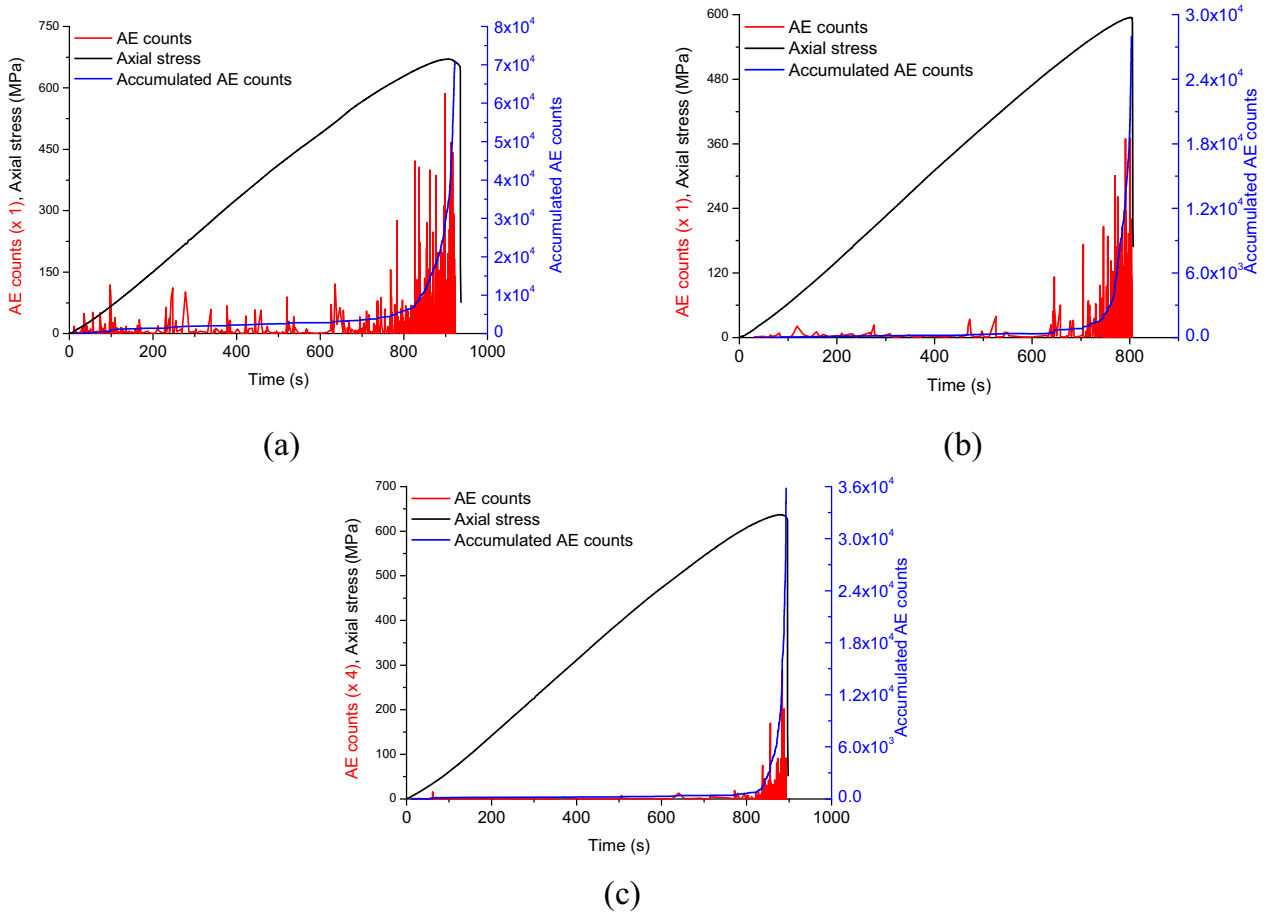


**Figure 13.** AE hit rate and cumulative AE ringing count curves of rock samples under triaxial stress conditions ( $P_c = 50$  MPa): (a) dry; (b) saturated with nano-emulsion; (c) saturated with distilled water.

denotes angle of internal friction. Based on the stress–strain curve at different confining pressures, the Mohr–Coulomb failure envelope between dry and fluid-saturated samples was determined (Fig. 17). Figure 17 shows that fluid saturation makes failure envelope to move downward, which promotes crack propagation along the plane of weakness. The failure envelope of nano-emulsion saturated sample was lower than that of the sample saturated with distilled water, indicating that nano-emulsion fluid is more advantageous for promoting crack propagation in hydraulic fracturing. The parameters of the Mohr–Coulomb criterion between dry and saturated samples are listed in Table 2. We observed that fluid saturation decreases the cohesion and angle of internal friction of rocks. It merits noting that both dry and fluid-saturated samples satisfy the Mohr–Coulomb criterion, although the

cohesive strength and internal friction angle of rocks were changed by fluid saturation.

### b-Value Analysis

When studying seismic activity, Gutenberg and Richter (1950) proposed the famous statistical relationship between earthquake magnitude and frequency, thus:

$$\lg N = a - bM, \quad (6)$$

where  $N$  is earthquake magnitude,  $M$  is number of earthquakes with magnitude between  $M$  and  $M + \Delta M$ , which is defined by logarithm of AE amplitude, i.e.,  $\lg A$ , and  $a$  and  $b$  are constants. The  $b$ -value, which is derived from the slope of the  $\lg N$ – $\lg A$  plot, is positive (Fig. 18a). We observed that

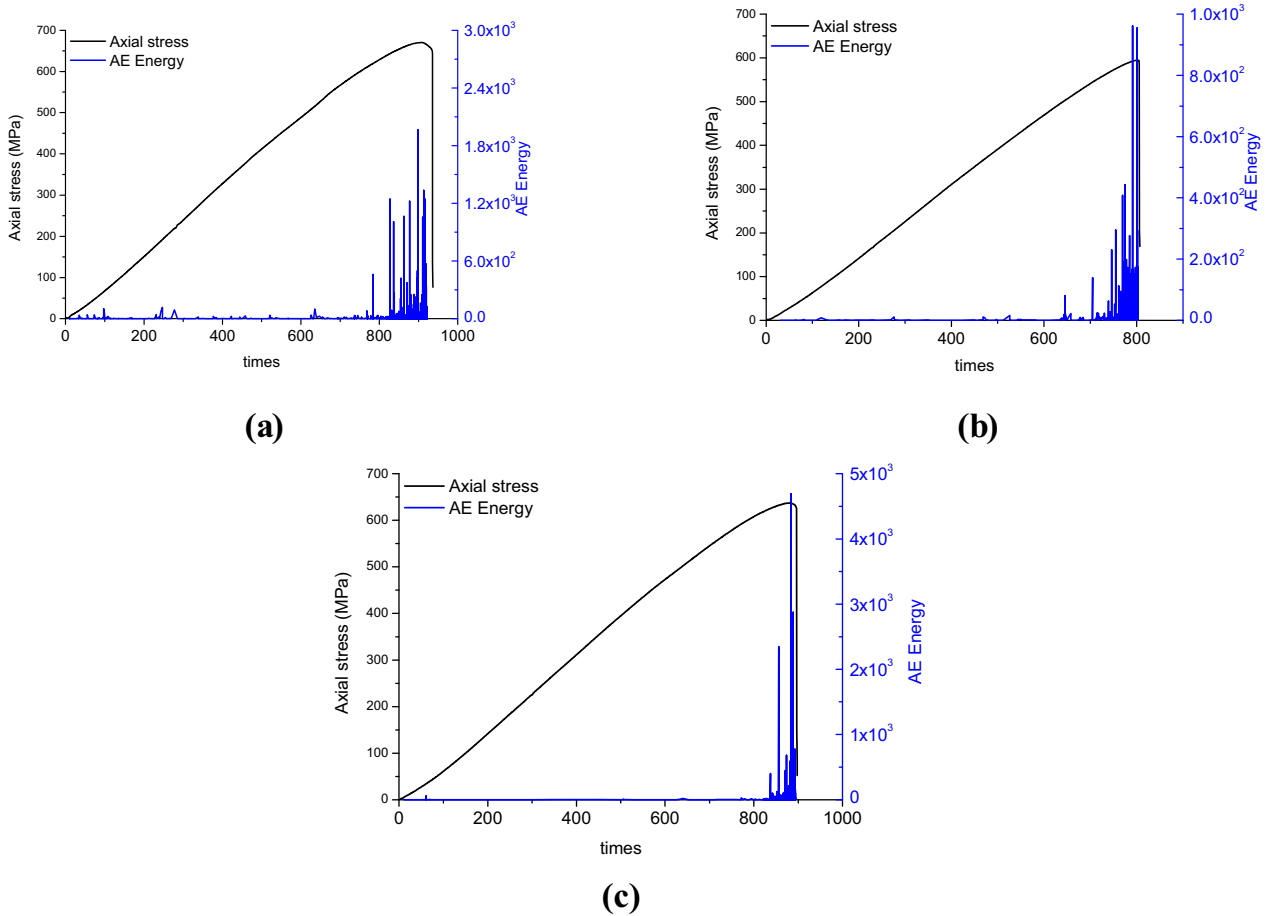


Figure 14. AE energy curves of rock samples under triaxial stress conditions ( $P_c = 50$  MPa): (a) dry; (b) saturated with nano-emulsion; (c) saturated with distilled water.

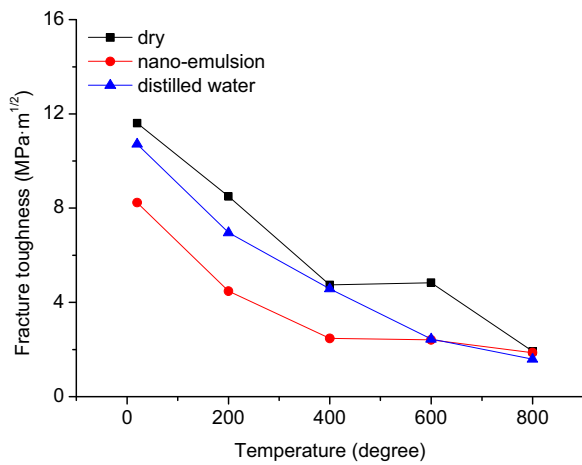


Figure 15. Comparison of fracture toughness between fluid-saturated and dry rock samples.

there was a good linear relationship between  $\lg N$  and  $\lg A$ , and hence, the determined  $b$ -value was very reliable.

Figure 18b shows that the  $b$ -value of fluid-saturated sample was much less than that of dry sample, which indicates that fluid promotes AE activity in rocks. In the early stage of loading, the  $b$ -value of fluid-saturated sample fluctuated many times, showing that micro-crack propagation occurred in fluid-saturated samples.

### Frequency Spectrum Analysis

To obtain more useful information from AE signals (e.g., frequency of main amplitude and energy distribution), frequency analysis is a very powerful signal processing technology. Based on the

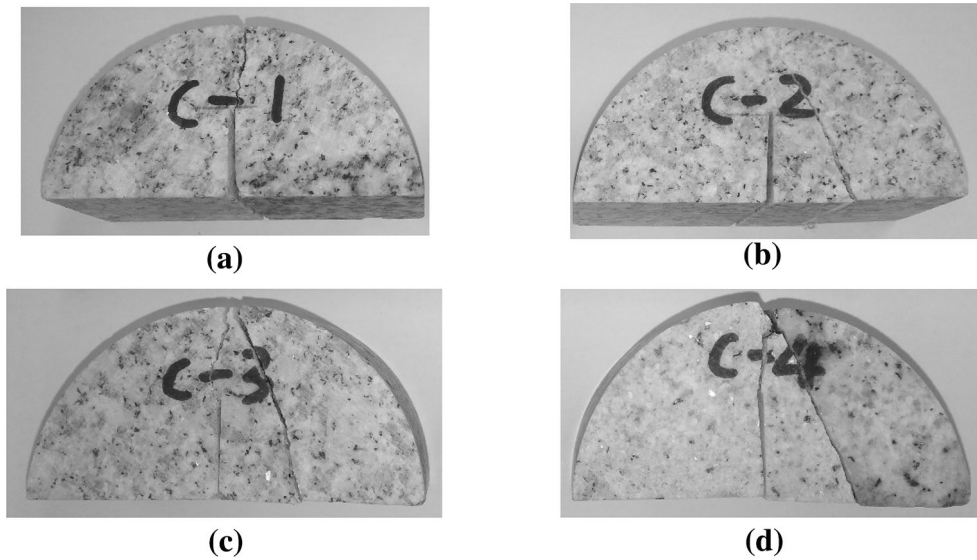


**Figure 16.** Fracture morphologies of semicircular bending test between fluid-saturated and dry rock samples: (a) dry; (b) saturated with nano-emulsion; (c) saturated with distilled water.

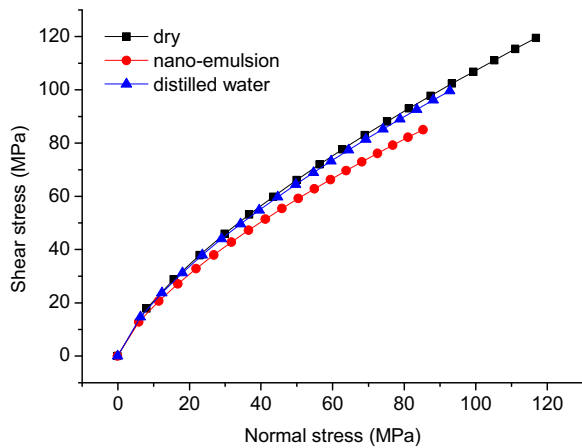


**Figure 17.** Comparison of failure envelopes between dry and fluid-saturated rock samples.

AE waveforms at different stress levels, frequency spectrum can be obtained by fast Fourier transform (FFT) algorithm. Figure 19 shows that the main frequency of dry sample was about 75 kHz at different percentages of failure load, i.e., 10%, 50% and 90% failure load. However, the main frequency of fluid-saturated samples became larger as the failure load increased. This is very consistent with the results shown in Figures 10, 11 and 15, indicating that our experimental results were reliable. In addition, the frequency spectrum curves of dry sample at different stress levels were getting close to

**Table 2.** Comparison of parameters of Mohr–Coulomb criterion between dry and saturated samples

Sample	Cohesion (MPa)	Angle of internal friction (degree)
Dry	16.74	44.45
Distilled water	13.71	42.97
Nano-emulsion	12.03	42.22

each other, while that of the fluid-saturated samples was separated as the stress level increased. This separation shows that AE energy is released at elevated loads due to micro-cracking induced by fluids.

### CONCLUSIONS

In this paper, a series of laboratory experiments were carried out on a servo-controlled triaxial rock mechanics apparatus to investigate mechanical properties and failure mechanisms of fluid-saturated hot dry rocks, combined with ultrasound measurement and AE monitoring. This study provides a better understanding of the mechanisms of complex fracture formation in hydraulic fracturing of geothermal reservoirs. Fluid saturation can weaken the cementation strength between mineral grains in hot dry rocks, and thus can decrease the key

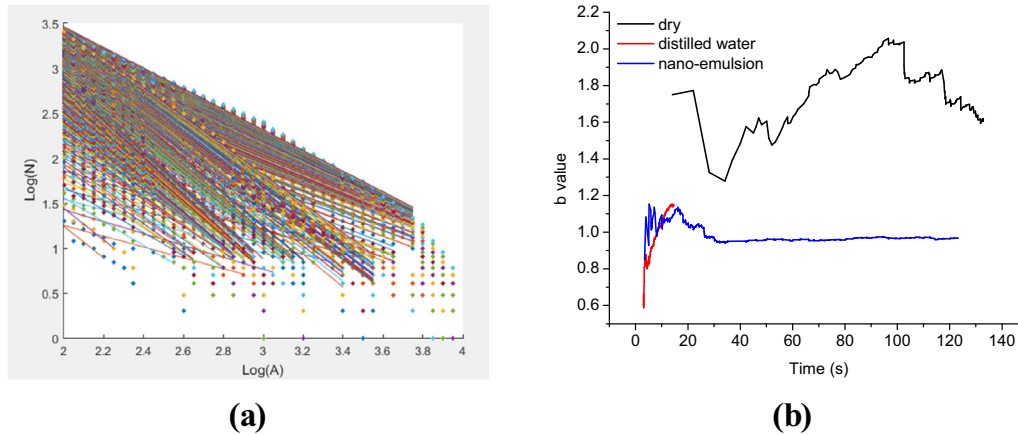


**Figure 18.** Comparison of  $b$ -value between dry and saturated samples: (a) linear relationship between  $\log N$  and  $\log A$ ; and (b)  $b$ -value.

mechanical parameters, including elastic moduli, crack damage stress ratio, compression strength, fracture toughness, cohesive strength and angle of internal friction both under uniaxial and triaxial stress conditions.

Fluid type has a significant effect on crack propagation of saturated hot dry rock samples. Our experimental results show that the crack damage stress ratio for nano-emulsion saturation was about 4–8% less than that for distilled water saturation. Nano-emulsion is more beneficial than distilled water for promoting the propagation of preexisting micro-cracks in rock samples.

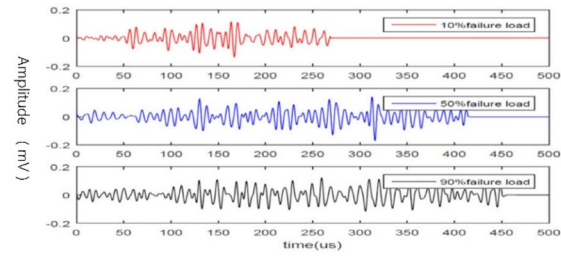
The increase ratio of longitudinal wave velocity of fluid-saturated rock samples was about 40% more than that of dry rock samples. The free water inside rock samples increases pore pressure in rocks, which further promotes crack initiation, propagation and coalescence in hydraulic fracturing of geothermal reservoirs.

Rock deformation is quite different between dry and fluid-saturated samples. The value of crack

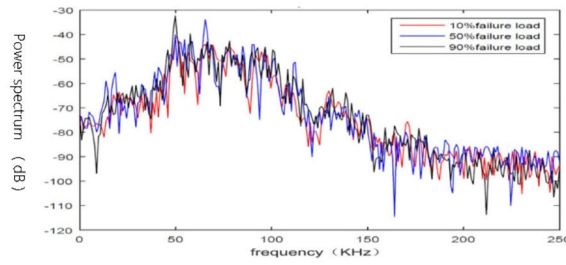
damage stress ratio decreased by about 4% upon saturation. This indicates that rock failure for fluid-saturated samples was slightly earlier than for dry samples.

The AE characteristics were quite different between dry and fluid-saturated samples. AE energy and AE hit rate of fluid-saturated sample were higher than those of dry sample. Many step-like jumps appeared on the curve of cumulative AE ringing counts of saturated sample, showing that fluid saturation can promote micro-crack initiation, propagation and nucleation in rock samples.

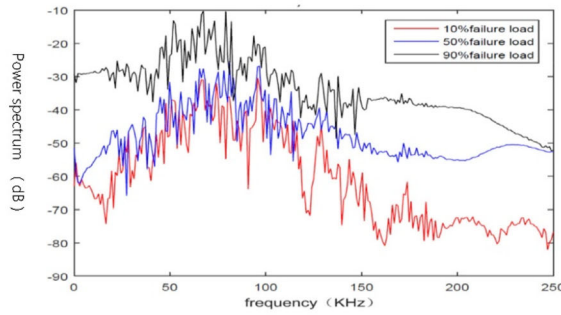
Fracture envelope,  $b$ -value of AE event and frequency spectrum were analyzed in detail to compare the failure mechanisms between dry and saturated samples. Fluid-saturated samples were characterized by lower fracture envelope, smaller  $b$ -value and separated frequency spectrum with different main frequencies. The order of enhancing fracture complexity was nano-emulsion saturation, distilled water saturation and dry sample.



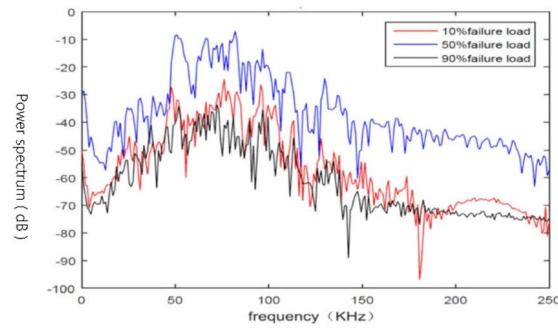
(a)



(b)



(c)



(d)

**Figure 19.** Characteristics of frequency spectrum between saturated and dry sample: (a) AE waveforms; (b) dry; (c) nano-emulsion; and (d) distilled water.

## ACKNOWLEDGMENTS

This work is financially supported by the National Science Foundation of China (Grant Nos. 51804033 and 51936001), and Jointly Projects of Beijing Natural Science Foundation, and Beijing Municipal Education Commission (Grant No. KZ201810017023).

## REFERENCES

- Althaus, E., Friz-Töpfer, A., Lempp, Ch., & Natau, O. (1994). Effects of water on strength and failure mode of coarse-grained granites at 300°C. *Rock Mechanics and Rock Engineering*, 27(1), 1–21.
- ASTM D8044–16. (2016). *Standard test method for evaluation of asphalt mixture cracking resistance using the semi-circular bend test (SCB) at intermediate temperatures*. West Conshohocken: ASTM International. <https://doi.org/10.1520/D8044-16>.
- Atkinson, B. K. (1987). *Fracture mechanics of rock*. London: Department of Geological Sciences, University College London, Elsevier. <https://doi.org/10.1016/C2009-0-21691-6>.
- Bai, M., Reinicke, K. M., Teodoriu, C., & Fichter, C. (2012). Investigation on water–rock interaction under geothermal hot dry rock conditions with a novel testing method. *Journal of Petroleum Science and Engineering*, 90–91, 26–30.
- Bauer, S. J., & Handin, J. (1983). Thermal expansion and cracking of three confined water-saturated igneous rocks to 800°C. *Rock Mechanics and Rock Engineering*, 16(3), 181–198.
- Cai, M., Kaiser, P. K., Tasaka, Y., Maejima, T., Morioka, H., & Minami, M. (2004). Generalized crack initiation and crack damage stress thresholds of brittle rock masses near underground excavations. *International Journal of Rock Mechanics and Mining Sciences*, 41(5), 833–847.
- Chaki, S., Takarli, M., & Agbodjan, W. P. (2008). Influence of thermal damage on physical properties of a granite rock: Porosity, permeability and ultrasonic wave evolutions. *Construction and Building Materials*, 22(7), 1456–1461.
- Dai, F., Wei, M. D., Xu, N. W., Zhao, T., & Xu, Y. (2015). Numerical investigation of the progressive fracture mechanisms of four ISRM-suggested specimens for determining the mode I fracture toughness of rocks. *Computers and Geotechnics*, 69, 424–441.
- Evans, K. F., Moriya, H., Niitsuma, H., Jones, R. H., Phillips, W. S., Genter, A., et al. (2005). Microseismicity and permeability enhancement of hydrogeologic structures during massive fluid injections into granite at 3 km depth at the Soultz HDR site. *Geophysical Journal International*, 160(1), 388–412.
- Fjar, E., Holt, R. M., Raaen, A. M., Horsrud, P., & Risnes, R. (2008). *Petroleum related rock mechanics* (2nd ed., Vol. 53). Amsterdam: Elsevier Science.
- Gong, H., Wang, B., Liang, H., Luo, Z., & Cao, Y. (2020). Strategic analysis of China's geothermal energy industry. *Frontiers of Engineering Management*. <https://doi.org/10.1007/s42524-020-0106-4>.
- Gringarten, A. C., Witherspoon, P. A., & Ohnishi, Y. (1975). Theory of heat extraction from fractured hot dry rock. *Journal of Geophysical Research* (1896–1977), 80(8), 1120–1124.
- Guo, T., Gong, F., Wang, X., Lin, Q., Qu, Z., & Zhang, W. (2019). Performance of enhanced geothermal system (EGS) in fractured geothermal reservoirs with CO<sub>2</sub> as working fluid. *Applied Thermal Engineering*, 152, 215–230.
- Guo, T., Zhang, S., Ge, H., Wang, X., Lei, X., & Xiao, B. (2015). A new method for evaluation of fracture network formation capacity of rock. *Fuel*, 140, 778–787.
- Gutenberg, B., & Richter, C. F. (1950). Seismicity of the earth and associated phenomena. *Bulletin of the Seismological Society of America*, 40(1), 76.
- Hasan, A. S. M., Osman, N. M., Ismail, M. K. A., Albar, A., & Razali, M. (2019). Rock water interaction on the effect of drying and wetting to the mechanical and dynamic properties of tropical weathered granite. *Journal of Physics: Conference Series*, 1349, 012070.
- Jupe, A. J., Green, A. S. P., & Wallroth, T. (1992). Induced microseismicity and reservoir growth at the Fjällbacka hot dry rocks project, Sweden. *International Journal of Rock Mechanics and Mining Sciences and Geomechanics Abstracts*, 29(4), 343–354.
- Kahraman, S. (2007). The correlations between the saturated and dry P-wave velocity of rocks. *Ultrasonics*, 46(4), 341–348. <https://doi.org/10.1016/j.ultras.2007.05.003>.
- Kohl, T., Evansi, K. F., Hopkirk, R. J., & Rybach, L. (1995). Coupled hydraulic, thermal and mechanical considerations for the simulation of hot dry rock reservoirs. *Geothermics*, 24(3), 345–359.
- Lockner, D. (1993). The role of acoustic emission in the study of rock fracture. *International Journal of Rock Mechanics and Mining Sciences and Geomechanics Abstracts*, 30(7), 883–899.
- Menéndez, B., David, C., & Darot, M. (1999). A study of the crack network in thermally and mechanically cracked granite samples using confocal scanning laser microscopy. *Physics and Chemistry of the Earth, Part A: Solid Earth and Geodesy*, 24(7), 627–632.
- Mignan, A., Landtwing, D., Kästli, P., Mena, B., & Wiemer, S. (2015). Induced seismicity risk analysis of the 2006 Basel, Switzerland, enhanced geothermal system project: Influence of uncertainties on risk mitigation. *Geothermics*, 53, 133–146.
- Nejati, M., Aminzadeh, A., Saar, M. O., & Driesner, T. (2019). Modified semi-circular bend test to determine the fracture toughness of anisotropic rocks. *Engineering Fracture Mechanics*, 213, 153–171.
- Nur, A., & Simmons, G. (1969). The effect of saturation on velocity in low porosity rocks. *Earth and Planetary Science Letters*, 7(2), 183–193.
- Pauwels, H., Fouillac, C., & Criaud, A. (1992). Water-rock interactions during experiments within the geothermal hot dry rock borehole GPK1, Soultz-sous-Forêts, Alsace, France. *Applied Geochemistry*, 7(3), 243–255.
- Richards, H. G., Savage, D., & Andrews, J. N. (1992). Granite-water reactions in an experimental hot dry rock geothermal reservoir, Rosemanowes test site, Cornwall, UK. *Applied Geochemistry*, 7(3), 193–222.
- Wan, Z., Zhao, Y., & Kang, J. (2005). Forecast and evaluation of hot dry rock geothermal resource in China. *Renewable Energy*, 30(12), 1831–1846.
- Wang, D., Ge, H., Wang, X., Wang, J., & Meng, F. (2015). The mechanical properties of gas shale under uniaxial stress. In *Presented at the 13th ISRM international congress of rock mechanics, international society for rock mechanics and rock engineering*, 10–13 May, Montreal, Canada. <https://www.onepetro.org/conference-paper/ISRM-13CONGRESS-2015-037>.
- Wang, D., Ge, H., Wang, X., Wang, J., Meng, F., Suo, Y., et al. (2015b). A novel experimental approach for fracability evaluation in tight-gas reservoirs. *Journal of Natural Gas Science and Engineering*, 23, 239–249.
- Wang, D., Wang, X., Ge, H., Sun, D., & Yu, B. (2020a). Experimental study on the failure mechanisms in brittle shales. *ACS Omega*, 5(18), 10382–10394.



- Wang, D., Wang, X., Ge, H., Sun, D., & Yu, B. (2020b). Insights into the effect of spontaneous fluid imbibition on the formation mechanism of fracture networks in brittle shale: An experimental investigation. *ACS Omega*, 5(15), 8847–8857.
- Wang, T., Ye, X., Liu, Z., Gao, Y., & Zhuang, Z. (2019a). An optimized perforation clusters spacing model based on the frictional shale layer. *Science China Physics, Mechanics and Astronomy*, 62(11), 114621.
- Wang, D., Yu, B., Qin, H., Yan, X., Cheng, W., Liu, Q., et al. (2019). An experimental study on the fracability evaluation of hot dry rock: Using an integrated thermo-mechanical model. In *Presented at the ISRM 14th international congress of rock mechanics*. Foz do Iguassu, Brazil: Rock Mechanics for Natural Resources and Infrastructure Development.
- Wang, D., Yu, B., Yan, X., Sun, D., Han, D., Qin, H., & Zhang, W. (2019). An experimental study on the fracture mechanics characteristics of heat-treated hot dry rock samples under different loading rates. In *Presented at the 53rd U.S. rock mechanics/geomechanics symposium, American rock mechanics association*, 23–26 June, New York City, New York. <https://www.onepetro.org/conference-paper/ARMA-2019-0120>.
- Wang, D., Zhou, F., Dong, Y., Sun, D., & Yu, B. (2020c). Experimental investigation of thermal effect on fracability index of geothermal reservoirs. *Natural Resources Research*. <https://doi.org/10.1007/s11053-020-09733-0>.
- Wang, D., Zlotnik, S., Diez, P., Ge, H., Zhou, F., & Yu, B. (2020d). A numerical study on hydraulic fracturing problems via the proper generalized decomposition method. *CMES-Computer Modeling in Engineering and Sciences*, 122(2), 703–720.
- Xie, L., Min, K.-B., & Song, Y. (2015). Observations of hydraulic stimulations in seven enhanced geothermal system projects. *Renewable Energy*, 79, 56–65.
- Yang, R., Huang, Z., Shi, Y., Yang, Z., & Huang, P. (2019). Laboratory investigation on cryogenic fracturing of hot dry rock under triaxial-confining stresses. *Geothermics*, 79, 46–60.
- Yang, S.-Q., Ranjith, P. G., Jing, H.-W., Tian, W.-L., & Ju, Y. (2017). An experimental investigation on thermal damage and failure mechanical behavior of granite after exposure to different high temperature treatments. *Geothermics*, 65, 180–197.
- Yu, Q. L., Ranjith, P. G., Liu, H. Y., Yang, T. H., Tang, S. B., Tang, C. A., et al. (2015). A mesostructure-based damage model for thermal cracking analysis and application in granite at elevated temperatures. *Rock Mechanics and Rock Engineering*, 48(6), 2263–2282.
- Zhang, F., Hu, D. W., Xie, S. Y., & Shao, J. F. (2014). Influences of temperature and water content on mechanical property of argillite. *European Journal of Environmental and Civil Engineering*, 18(2), 173–189.
- Zhang, F., Zhao, J., Hu, D., Skoczylas, F., & Shao, J. (2018). Laboratory investigation on physical and mechanical properties of granite after heating and water-cooling treatment. *Rock Mechanics and Rock Engineering*, 51(3), 677–694.
- Zhang, L., Zhou, F., Mou, J., Pournik, M., Tao, S., Wang, D., et al. (2019). Large-scale true tri-axial fracturing experimental investigation on diversion behavior of fiber using 3D printing model of rock formation. *Journal of Petroleum Science and Engineering*, 181, 106171.
- Zhao, Y., Feng, B., Zhang, G., Shangguan, S., Qi, X., Li, X., et al. (2020). Study of the interaction between the granitic hot-dry rock (HDR) and different injection waters. *Acta Geologica Sinica*, 94(07), 2115–2123.
- Zhou, Z., Cai, X., Zhao, Y., Chen, L., Xiong, C., & Li, X. (2016). Strength characteristics of dry and saturated rock at different strain rates. *Transactions of Nonferrous Metals Society of China*, 26(7), 1919–1925.
- Zhuang, L., Kim, K. Y., Diaz, M., & Yeom, S. (2020). Evaluation of water saturation effect on mechanical properties and hydraulic fracturing behavior of granite. *International Journal of Rock Mechanics and Mining Sciences*, 130, 104321.